buildings

MDPI

Article

A Statistical Experimental Design Using Response Surface Methodology for High-Performance Lightweight Concretes Containing Pumice Aggregate

Esra Tugrul Tunc *, Kursat Esat Alyamac, Ragip Ince and Zulfu Cinar Ulucan

Civil Engineering Department, Engineering Faculty, Firat University, 23119 Elazig, Turkey; kealyamac@firat.edu.tr (K.E.A.); rince@firat.edu.tr (R.I.); zculucan@firat.edu.tr (Z.C.U.)
* Correspondence: esratugrul@firat.edu.tr

Abstract

It is possible to reduce the self-weight of buildings by using high-performance lightweight concretes (HPLCs) instead of conventional concrete. It is known that many provinces of Turkey are in dangerous earthquake zones. In this context, one of the most appropriate ways to reduce the self-weight of buildings, in terms of minimizing earthquake damages, is to use lightweight concrete. Due to the increasing need for HPLCs today, the related study draws attention to this aspect. In the present study, it is planned to evaluate the fresh and hardened concrete properties of HPLCs produced with pumice aggregates in two stages, experimentally and statistically. In the first stage, a 28-day series of HPLCs with different mix ratios and different concrete components was produced. Fresh and hardened concrete properties, such as slump and strength of the produced HPLCs, were determined. As a result of the experiments, all results for each concrete recipe were examined comparatively, and the best concrete recipes were determined. Then, in the second stage, after the experiments were completed, the slump, compressive strength, and splitting tensile strength of HPLCs were analyzed with the multi-objective optimization method using the Response Surface Method. With these developed equations, it was observed that the machinability and strength properties of HPLCs for different test parameters were predicted with high accuracy. Consequently, developing HPLC mix designs through this predictive approach significantly reduces experimental workload, leading to substantial savings in labor, time, and costs.

Keywords: high-performance lightweight concrete (HPLC); pumice aggregate; slump; compressive strength; response surface method (RSM)

Check for updates

Academic Editor: Xiaoyong Wang

Received: 18 June 2026
Revised: 18 July 2026
Accepted: 19 July 2026
Published: 22 July 2026

Copyright: © 2026 by the authors. Licensee MDPI, Basel, Switzerland. This article is an open access article distributed under the terms and conditions of the Creative Commons Attribution (CC BY) license.

1. Introduction

Since concrete production is easy and directly affects the performance of buildings, the mixture should be designed very carefully and in accordance with the intended use [1,2]. One of the most important factors affecting concrete strength is aggregate [3,4]. Aggregate directly affects many properties of concrete, such as workability, strength and permeability [5–7]. The most important feature required from concrete, in accordance with its intended use, is high strength. That is, it must be resistant to physical/chemical external effects [8,9]. Durable concrete should resist loads without deforming or breaking. The maximum value of this resistance determines concrete strength [10]. High-strength concrete is defined as concrete with a compressive strength of 55 MPa and above according to ACI

363R-10 [11]. In the current study, the aim is to obtain strengths of around 80–90 MPa. Concrete strength is also a parameter that determines other properties of concrete. For this reason, concretes are classified based on their compressive strength in relevant standards. Important factors affecting the compressive strength of concrete are aggregate properties (aggregate type, granulometry, shape, size, etc.), cement content, the water–cement ratio, workability, additive type and amount, and curing time [12–14].

Advances in the concrete industry show that concrete with different properties is needed with developing technology. With these innovations, concrete types classified as special concretes have begun to be investigated. Lightweight concrete is a type of concrete obtained by using lightweight aggregates. According to ACI 213R-87 [15], concretes with compressive strengths of up to 6.89 MPa are defined as low-density lightweight concretes, 6.89–17.24 MPa as medium-strength concretes (filling concretes), and those with 17.24–41.36 MPa and above as load-bearing lightweight concrete. Load-bearing lightweight concrete, which has been widely preferred especially in recent years, is a special type of concrete [16–18]. Load-bearing lightweight concretes have many advantages, especially technical, economic and environmental [19]. When a reinforced concrete structure is built using lightweight concrete, the total weight of the structure decreases, thereby decreasing the effect of horizontal forces in case of a possible earthquake. This helps prevent a significant amount of earthquake damage [20]. For this reason, it is very useful to build structures with lightweight concrete, especially in earthquake-prone areas [21]. In addition, because of the advantage of having more usable areas and openings in high-rise buildings, load-bearing light concrete is recommended [22].

While detailed structural dynamic simulations or full-scale building modeling are beyond the laboratory scope of this materials-centric investigation, the physical reduction in concrete density directly correlates with fundamental seismic demand formulations. According to structural design principles, the total seismic base shear (V_t) is a direct function of the structure's effective seismic weight (W_{ef}), expressed as $V_t = C_s \times W_{ef}$. The lightweight concrete formulations developed herein exhibit unit weights ranging from 1650 to 1900 kg/m^3, representing an approximate 20–30% dead load reduction compared to conventional normal-weight concrete (2400 kg/m^3). Consequently, this material-level weight mitigation mathematically ensures a proportional decrease in the structural mass inertial forces triggered during seismic excitations, shifting the claim from a declarative statement to a baseline structural dynamic mechanism [20–22].

High-performance lightweight concretes (HPLCs) have properties that are compatible with, or even improved compared to, conventional concrete (CC), but they are considerably lighter compared to conventional concrete. By using HPLC, it is possible to lighten buildings by reducing the total amount of concrete to be used [23,24]. By accurately determining the bearing properties of HPLCs, it is possible to determine the bearing capacities of structural systems such as beams, columns and walls as well as the behavior of bearing frames under lateral loads [25–27]. In addition, it has been found that the dead weight of a building and the area of reinforcement to be used decreases if lightweight aggregates are used in concrete. Today, increasing earthquake risk has increased interest in HPLCs [28,29].

Since Turkey is in an earthquake-prone zone and has experienced earthquakes that have caused significant financial losses and emotional suffering, it was thought that the dead load of buildings should be reduced. This can be achieved by using building materials produced with lightweight aggregates. Furthermore, building loads can be minimized without reducing their strength characteristics by producing lightweight concrete using lightweight aggregates [24]. Pumice, a lightweight aggregate, may be preferred in lightweight concrete production due to its abundant reserves globally and in Turkey [30,31]. The use of pumice as a building material is becoming more and more widespread [32,33].

Since concrete produced with pumice is lighter than normal concrete, time and labor savings are achieved [34–36]. However, chemical and mineral additives should be used together with pumice to produce HPLCs. Tuğrul Tunç et al. (2018), who developed a statistical method for determining the compressive strength of lightweight concretes produced using pumice aggregates and chemical additives, taking into account the literature, observed that the compressive strength of lightweight concretes varies between 14.18 MPa and 43.27 MPa [24].

Silica fume has been the most widely used mineral additive in the production of high-strength concrete [37,38]. It has been determined that the 28-day compressive strengths of concretes produced with silica fume vary between 30 MPa and 40 MPa [39]. Mortazavi et al. (2013) determined the compressive strength of structural lightweight concretes containing different proportions of silica fume by subjecting them to different curing times [40]. Bogas et al. (2014) aimed to produce silica-fume-reinforced lightweight concretes with superior thermal insulation properties in order to reduce energy consumption and heat transfer in buildings [41]. Previous experimental studies on the strength and durability properties of silica-fume-containing lightweight concretes were conducted by various researchers [42,43]. Due to the increasing need for HPLCs, the present study draws attention to this aspect. The fact that building floors are vulnerable to earthquake risk and that the building area will be exposed to natural events shows that the concrete to be produced should possess both strength and durability. This will only be possible with the production of HPLCs.

Although continuous research has evaluated the standalone mechanical performance of high-performance lightweight concretes (HPLCs) containing pumice aggregates [24], capturing the combined structural interactions between low-porosity cementitious matrices and industrial by-products remains a challenging objective. Prior empirical frameworks typically relied on single-variable experimental approaches, which fail to evaluate the interactive effects of multiple mix variables on overall concrete behavior. The present study addresses this research gap by employing comprehensive multi-objective optimization via Response Surface Methodology (RSM). By integrating four independent dimensionless parameters—the water-to-cement ratio, the aggregate-to-cement ratio, silica fume content, and waste marble dust substitution—this work models the mutual interaction mechanics governing concrete performance, moving beyond conventional empirical reporting to deliver precise predictive formulations. The distinct novelty of this approach stems from the concurrent modeling of alternative industrial by-products alongside cellular lightweight skeletons using precise dimensionless boundaries. Unlike linear empirical reports, this formulation explicitly captures the microstructural interaction boundaries where pozzolanic and crystalline filler kinetics counteract the intrinsic strength loss of porous pumice.

The aim of the present study is to determine the best mixtures of HPLCs, produced using pumice aggregates. For this purpose, in the first stage, a series of additive concrete mixtures with different dosages for different water–cement ratios were prepared by using different-sized pumice aggregates. Slump, 28-day compressive strength and splitting tensile strength tests of the produced HPLCs were carried out. All relevant results were compared, and the effects of aggregates containing pumice on concrete strength were investigated. In addition, the relationship between the compressive strength of HPLCs and the splitting tensile strength was also determined. Then, in the second stage, the mixture recipes of the HPLCs to be produced were analyzed using the Response Surface Method (RSM), which is one of the best optimization methods for determining the relationship between multiple factors and the response. The specific objective of this study is to determine and evaluate the performance boundaries of HPLCs using defined quantitative optimization criteria. The material optimization targets a minimum threshold workability (slump $\geq$ 10 cm) paired with high load-bearing capacity ($f_c \geq$ 55 MPa and up to 80–90 MPa) within a lightweight

structural density window (1650–1900 kg/m^3). Furthermore, the effectiveness and predictive accuracy of the developed response surface equations are systematically verified against target validation metrics, including a high coefficient of determination ($R^2 \geq 0.90$), non-significant Lack-of-Fit indexes, and absolute error margins strictly under 6% for independent confirmation configurations. With the help of experimental data, it is hoped that the equations obtained by the method developed using dimensionless parameters such as water–cement, aggregate–cement, silica fume–cement and marble dust–aggregate ratio can be used safely in the prototype. In addition, the use of pumice as an aggregate in the production of HPLCs in the current study will contribute to the economy due to its high reserves in Turkey.

2. Materials and Methods

2.1. Materials

In the present study, pumice aggregates from the Turkey–Bitlis–Ahlat region were used as lightweight aggregates for HPLC production (Figure 1a). Many researchers suggest limiting the maximum aggregate size (D_{max}) to 12.5 mm in the production of high-strength lightweight concrete, depending on the type of lightweight aggregate [44,45]. In this study, D_{max} = 8 mm was chosen to see the effects of aggregate maximum particle size. In lightweight aggregates, workability and strength decrease as the diameter increases. In the present study, the granulometry of the mix aggregates was determined according to the Fuller parabola [46]. The saturated dry surface specific gravity of the mixture aggregates was determined as 1.35 g/cm^3 according to ASTM C127 [47]; the water absorption ratio was determined as 20.8% according to ASTM C128-12 [48]; and the Los Angeles abrasion loss value was determined as 40% according to ASTM C131 [49]. In addition, limestone aggregates with D_{max} = 8 mm and the same adjusted granulometry were used as a reference for mixing aggregates to be used in HPLC production. In this study, the average saturated dry surface specific gravity of the limestone mix aggregates was determined as 2.68 g/cm^3, the water absorption rate was 1.2% and the Los Angeles abrasion loss value was 25%.

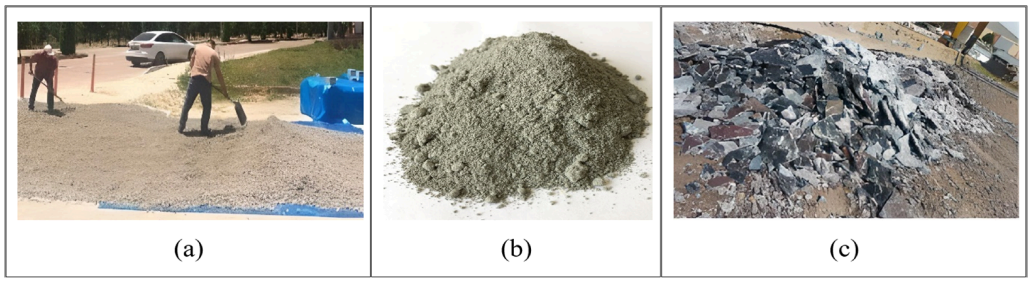


Figure 1. Materials used in HPLC production within the scope of the current study: (**a**) pumice aggregate, (**b**) silica fume, (**c**) waste marble aggregate.

CEM I 42.5 R Portland cement was used in the present experimental study. The specific gravity of this cement is 3.12 g/cm^3, and the Blaine specific surface area is 3490 cm^2/g. The initial setting time of the cement was determined as 2.8 h and the final setting time as 3.3 h. In addition, 2-day, 7-day, and 28-day compressive strengths of the cement mortar were determined as 29.5 MPa, 38.1 MPa and 61.5 MPa, respectively, in accordance with TS EN 197-1 [50]. In order to determine how the physical and mechanical properties of the produced HPLC samples change with changes in the amount of binder, concrete was produced for 4 different cement dosages: 400, 500, 600 and 700 kg/m^3.

In high-strength lightweight concretes, it is recommended to use silica fume or fly ash together with cement to strengthen the cement matrix. The purpose of using these pozzolanic materials is to increase ultimate strength and machinability [51]. In the present

study, silica fume with a specific gravity of 2.50 g/cm^3, a Blaine specific surface area of 296,000 cm^2/g and a glow loss of 1.68% was used as the mineral additive (Figure 1b). In this study, 0%, 8%, 16%, and 24% silica fume was added to the cement to increase the amount of fine powder material, and the effect of the added silica fume on the fresh and hardened concrete properties of HPLCs was investigated.

In the present experimental study, marble powder obtained from the waste of sour cherry marble extracted in the province of Turkey–Elazig was used (Figure 1c). The specific gravity of the waste marble powder is 2.70 g/cm^3, and the Blaine specific surface area is 3924 cm^2/g. In this study, 0%, 8%, 16% and 24% waste marble powder were added to cement for concrete mixes with a 50% fine aggregate ratio, and the effect of the added waste marble powder on the fresh and hardened concrete properties of HPLCs was investigated. By including waste marble dust in concrete production, we aim to reduce industrial waste accumulation, support resource efficiency and improve concrete properties. Thus, this will contribute to both the marble sector and the national economy. In addition, recycling practices will support the environment and human health [52–54].

Since the water–cement ratios are low in the current experimental studies, a new-generation polycarboxylate-supported superplasticizer was used to ensure workability and prevent decomposition [55]: liquid, brown, density 1.075 $\pm$ 0.02 g/cm^3, pH 4.00 $\pm$ 1 and chloride content < 0.1%. In this study, chemical additives up to 1.2% of cement weight were added to HPLC mixtures for different dosages (C = 400, 500, 600 and 700 kg/m^3).

To counteract the high water absorption capacity of the porous pumice aggregate and maintain strict control over the effective water-to-cement ratio, the aggregates were brought to a Saturated-Surface-Dry (SSD) condition prior to the mixing process. The coarse and fine pumice particles were pre-soaked in water for 24 h, subsequently spread on a clean surface, and air-dried until the glossy water film disappeared from the aggregate surfaces. This pre-conditioning methodology prevents the porous aggregate skeleton from absorbing the net mixing water from the fresh matrix, thereby ensuring the accuracy and reproducibility of the designated W/C ratios across all concrete compositions.

2.2. Method and Tests

In order to determine the fresh concrete properties of HPLCs, 60 slump tests were performed for each series in accordance with ASTM C143 [56] (Figure 2a). Fresh concrete was filled into cube molds of 150 $\times$ 150 $\times$ 150 mm (Figure 2b). The slump values obtained from the study are given in the test results section, and the conformity of the produced HPLCs to the consistency class has been determined. Then, 150 $\times$ 150 $\times$ 150 mm specimens removed from the molds were kept in curing pools (Figure 2c). At the end of the 28-day curing period, using 3 samples for each batch, a compressive strength test (Figure 2d) in accordance with the TS EN 12390-3 [57] standard and a split tensile strength test (Figure 2e) in accordance with the TS EN 12390-6 [58] standard were performed for a total of 180 samples. The compressive and splitting tensile strengths obtained from the study are given as the arithmetic average of 3 concrete samples for each series in the test results section, and the effects of different parameters on the concrete strength are discussed in detail.

All concrete mixing operations were performed under controlled laboratory conditions at an ambient temperature of 20 $\pm$ 2 °C and a relative humidity of 50 $\pm$ 5%. The raw components were mixed in a laboratory-scale pan mixer using a systematic sequence: dry aggregates and cementitious materials were homogenized for 2 min, after which the net mixing water pre-blended with the superplasticizer was introduced, followed by an additional 3 min of intensive wet mixing to ensure full matrix homogeneity. The mechanical testing was carried out using a closed-loop servo-hydraulic compression machine. In strict accordance with TS EN 12390-3 and TS EN 12390-6 frameworks, the loading rate was

maintained at a constant stress rate of 0.6 MPa/s for the compressive strength tests and 0.05 MPa/s for the splitting tensile strength configurations until ultimate specimen failure.

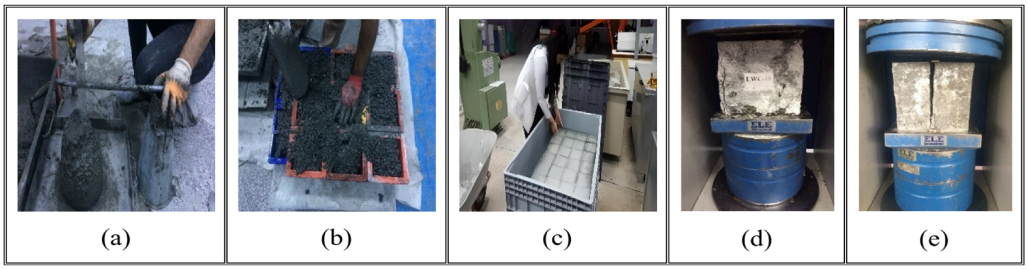


Figure 2. Performing the tests: (**a**) slump test, (**b**) fresh concrete placed in cube molds, (**c**) samples left in the curing pool, (**d**) compressive strength test for the hardened sample, (**e**) splitting tensile strength test for the hardened sample.

3. Experimental Study and Results

In the present study, 52 concrete recipes were prepared in order to obtain HPLCs using different-sized pumice aggregates and to determine the fresh and hardened concrete properties of the obtained HPLCs. In addition, eight concrete recipes were prepared in order to determine the fresh and hardened concrete properties of reference conventional concretes (CCs) produced using limestone aggregates of different sizes as a reference for HPLCs. Thus, a total of 60 concrete recipes, 52 HPLCs and 8 CCs, were prepared (Table 1). The concrete series containing pumice aggregates was expressed by HPLC, and the concrete series containing limestone aggregates was expressed as CC (normal concrete). In the prepared concrete recipes, change parameters, such as four different water–cement ratios (w/c = 0.25, 0.30, 0.35 and 0.40) and four different cement dosages (400, 500, 600 and 700 kg/m^3), were taken into consideration. In addition, the effect of silica fume and marble dust, which were used in the concrete recipes, on the physical and mechanical properties of the concrete to be obtained was one of the research subjects of the study.

Table 1. Mix recipes of HPLC samples.

Sample Code	*w/c* (-)	*w/b* (-)	C (kg/m^3)	SF (%)	WMD (%)	SP (%)	AC (kg)				
							0–1 (mm)	1–2 (mm)	2–4 (mm)	4–8 (mm)	8–16 (mm)
HPLC-1	0.25	0.25	400	0	0	1.2	294.3	213.1	152.2	101.5	253.7
HPLC-2	0.25	0.22	400	8	8	1.2	284.7	206.1	147.2	98.2	245.4
HPLC-3	0.25	0.20	400	16	8	1.2	279.7	202.5	144.7	96.4	241.1
HPLC-4	0.25	0.25	500	0	0	1.2	272.0	197.0	140.7	93.8	234.5
HPLC-5	0.25	0.22	500	8	8	1.2	259.9	188.2	134.4	89.6	224.1
HPLC-6	0.25	0.19	500	16	16	1.2	247.9	179.5	128.2	85.5	213.7
HPLC-7	0.25	0.25	600	0	0	1.2	249.7	180.8	129.1	86.1	215.2
HPLC-8	0.25	0.22	600	8	8	1.2	235.2	170.3	121.6	81.1	202.7
HPLC-9	0.25	0.20	600	16	8	1.2	227.7	164.9	117.8	78.5	196.3
HPLC-10	0.25	0.18	600	24	16	1.2	213.2	154.4	110.3	73.5	183.8
HPLC-11	0.25	0.25	700	0	0	1.2	227.3	164.6	117.6	78.4	196.0
HPLC-12	0.25	0.19	700	16	16	1.2	193.5	140.2	100.1	66.7	166.8

Table 1. *Cont.*

Sample Code	*w/c* (-)	*w/b* (-)	C (kg/m^3)	SF (%)	WMD (%)	SP (%)	AC (kg)				
							0–1 (mm)	1–2 (mm)	2–4 (mm)	4–8 (mm)	8–16 (mm)
CC-1	0.25	0.25	400	0	0	1.2	584.3	423.1	302.2	201.5	503.7
CC-2	0.25	0.25	500	0	0	1.2	540.0	391.0	279.3	186.2	465.5
CC-3	0.25	0.25	700	0	0	1.2	451.3	326.8	233.4	155.6	389.0
HPLC-13	0.30	0.30	400	0	0	1.2	286.5	207.5	148.2	98.8	247.0
HPLC-14	0.30	0.26	400	0	16	1.2	277.4	200.7	143.4	95.6	239.0
HPLC-15	0.30	0.24	400	8	16	1.2	272.2	197.1	140.8	93.9	234.7
HPLC-16	0.30	0.23	400	16	16	1.2	267.2	193.5	138.2	92.1	230.3
HPLC-17	0.30	0.21	400	24	16	1.2	262.2	189.9	135.6	90.4	226.0
HPLC-18	0.30	0.26	500	0	16	1.2	250.6	181.5	129.6	86.4	216.0
HPLC-19	0.30	0.24	500	16	8	1.2	243.9	176.6	126.1	84.1	210.2
HPLC-20	0.30	0.21	500	24	16	1.2	231.8	167.9	119.9	79.9	199.8
HPLC-21	0.30	0.30	600	0	0	1.2	237.9	172.3	123.1	82.0	205.1
HPLC-22	0.30	0.28	600	8	0	1.2	230.4	166.8	119.2	79.4	198.6
HPLC-23	0.30	0.24	600	8	16	1.2	216.5	156.8	112.0	74.6	186.6
HPLC-24	0.30	0.23	600	16	16	1.2	209.0	151.3	108.1	72.1	180.1
HPLC-25	0.30	0.21	600	24	16	1.2	201.4	145.9	104.2	69.5	173.7
HPLC-26	0.30	0.24	700	16	8	1.2	188.0	136.1	97.2	64.8	162.0
HPLC-27	0.30	0.21	700	24	16	1.2	171.1	123.9	88.5	59.0	147.5
CC-4	0.30	0.28	600	8	0	1.2	457.4	331.2	236.6	157.7	394.3
HPLC-28	0.35	0.30	400	8	8	1.2	269.0	194.8	139.1	92.8	231.9
HPLC-29	0.35	0.27	400	16	16	1.2	259.4	187.8	134.2	89.4	223.6
HPLC-30	0.35	0.27	500	8	24	1.2	228.8	165.6	118.3	78.9	197.2
HPLC-31	0.35	0.27	500	16	16	1.2	228.3	165.3	118.1	78.7	196.8
HPLC-32	0.35	0.25	500	24	16	1.2	222.0	160.8	114.8	76.6	191.4
HPLC-33	0.35	0.30	600	8	8	1.2	211.7	153.3	109.5	73.0	182.5
HPLC-34	0.35	0.27	600	16	16	1.2	197.2	142.8	102.0	68.0	170.0
HPLC-35	0.35	0.27	700	8	24	1.2	166.8	120.8	86.3	57.5	143.8
HPLC-36	0.35	0.27	700	16	16	1.2	166.1	120.3	85.9	57.3	143.2
HPLC-37	0.35	0.25	700	24	16	1.2	157.4	114.0	81.4	54.3	135.7
CC-5	0.35	0.27	400	16	16	1.2	514.9	372.9	266.3	177.5	443.9
HPLC-38	0.40	0.40	400	0	0	1.2	270.8	196.1	140.1	93.4	233.5
HPLC-39	0.40	0.30	400	16	16	1.2	251.5	182.1	130.1	86.7	216.8
HPLC-40	0.40	0.27	400	24	24	1.2	241.9	175.2	125.1	83.4	208.5
HPLC-41	0.40	0.40	500	0	0	1.2	242.6	175.7	125.5	83.7	209.2
HPLC-42	0.40	0.30	500	16	16	1.2	218.5	158.2	113.0	75.3	188.4
HPLC-43	0.40	0.27	500	24	24	1.2	206.4	149.5	106.8	71.2	178.0
HPLC-44	0.40	0.30	500	8	24	1.2	219.0	158.6	113.3	75.5	188.8

Table 1. *Cont.*

Sample Code	*w/c* (-)	*w/b* (-)	C (kg/m^3)	SF (%)	WMD (%)	SP (%)	AC (kg)				
							0–1 (mm)	1–2 (mm)	2–4 (mm)	4–8 (mm)	8–16 (mm)
HPLC-45	0.40	0.40	600	0	0	1.2	214.4	155.3	110.9	73.9	184.8
HPLC-46	0.40	0.30	600	16	16	1.2	185.5	134.3	95.9	64.0	159.9
HPLC-47	0.40	0.30	600	24	8	1.2	184.9	133.9	95.6	63.8	159.4
HPLC-48	0.40	0.27	600	24	24	1.2	171.0	123.8	88.4	59.0	147.4
HPLC-49	0.40	0.40	700	0	0	1.2	186.2	134.8	96.3	64.2	160.5
HPLC-50	0.40	0.30	700	8	24	1.2	153.1	110.9	79.2	52.8	132.0
HPLC-51	0.40	0.29	700	16	24	1.2	144.3	104.5	74.6	49.8	124.4
HPLC-52	0.40	0.29	700	24	16	1.2	143.7	104.0	74.3	49.5	123.8
CC-6	0.40	0.30	500	16	16	1.2	433.8	314.1	224.4	149.6	373.9
CC-7	0.40	0.30	600	24	8	1.2	367.1	265.8	189.9	126.6	316.5
CC-8	0.40	0.30	700	8	24	1.2	303.9	220.1	157.2	104.8	262.0

HPLC—high-performance lightweight concrete, CC—conventional concrete, *w/c*—water–cement ratio, *w/b*—water–binder ratio, C—cement content, SF—silica fume content, WMD—waste marble dust content, SP—superplasticizer chemical additive content and AC—aggregate content.

In terms of physical classification, the fresh density readings of the HPLC formulations shifted between 1710 kg/m^3 and 1860 kg/m^3 (±35 kg/m^3), while the 28-day oven-dry hardened densities systematically ranged between 1650 kg/m^3 and 1810 kg/m^3 (±42 kg/m^3). The lowest hardened density profile (1650 kg/m^3) was observed in the HPLC-38 batch (W/C = 0.40, without mineral additions), driven by the high capillary porosity left after excess moisture evaporation. Conversely, the upper structural lightweight density limit (1810 kg/m^3) was tracked in the high-dosage binder runs, such as HPLC-12 (W/C = 0.25, 16% SF, 16% WMD), where the physical micro-filler effect and pozzolanic matrix densification compacted the internal voids. These configurations strictly satisfy the maximum structural density threshold of 1840 kg/m^3 established by ACI 213R frameworks.

In terms of physical classification, the hardened oven-dry density of the produced HPLC mixtures systematically ranged between 1650 and 1900 kg/m^3. This physical weight mitigation yields an effective dead load reduction of approximately 21–33% relative to traditional normal-weight concrete 2400 kg/m^3, quantitatively validating the material's structural efficiency in seismic mass optimization. The hardened density of the produced HPLC specimens was determined at 28 days in accordance with TS EN 12390-7 [59]. Depending on the Response Surface Methodology (RSM) mix proportions—specifically driven by the water-to-cement and aggregate-to-cement ratios—the 28-day air-dry density of the concrete variations systematically ranged between 1510 kg/m^3 and 1645 kg/m^3, successfully satisfying the targeted design thresholds for structural lightweight components.

To verify the structural lightweight concrete qualification in accordance with ACI 213R, the physical density profiles of all manufactured mixtures were quantified. The fresh density readings of the HPLC formulations shifted between 1710 kg/m^3 and 1860 kg/m^3. Following the 28-day curing regime, the oven-dry hardened densities varied between 1650 kg/m^3 and 1810 kg/m^3. These density configurations strictly satisfy the maximum structural density threshold of 1840 kg/m^3 established by ACI 213R frameworks. The cellular micro-pore framework inherent to the Bitlis–Ahlat pumice structures successfully

reduced the dead weight by approximately 25–35% compared to the baseline conventional limestone concrete control series, confirming genuine lightweight structural optimization.

In addition to density profiles, the total air content configurations of the fresh HPLC mixtures were analyzed to track the internal void kinetics. The air content of the fresh HPLC mixtures was measured using the volumetric method, thereby mitigating the pressure-induced aggregate absorption errors typically associated with porous lightweight aggregates. The experimental matrix revealed that the fresh air content fluctuated between 2.8% and 6.2% across the 52 individual runs. The progressive reduction toward the lower bound (2.8%) was systematically observed in mixtures with maximum SF and WMD substitutions. This trend physically corroborates that the high specific surface area and intense micro-filling capacity of these mineral modifiers effectively densify the fresh matrix, thereby displacing the entrained air voids.

It is worth noting that the recorded fresh air content values (ranging from 2.8% to 6.8%) strictly signify entrapped air, given that no chemical air-entraining agents were utilized in this study. The upper limit of 6.8% is primarily attributed to the highly porous, angular, and rough surface morphology of the pumice aggregates, which increases internal friction during mixing and promotes the mechanical entrapment of air voids. However, this complex void system undergoes systematic alteration with the introduction of mineral modifiers. A clear direct correlation exists: as the combined SF and WMD content increased from 0% to its maximum substitution level, the air content systematically dropped from 6.8% to its minimum bound of 2.8%. This solid reduction confirms that the ultra-fine particle size distribution of SF and WMD counteracts the aggregate-induced air entrapment by filling the interstitial spaces between the lightweight aggregate particles. The structural baseline of these air void indexes is primarily driven by the highly cellular, multi-void mineralogy of the raw pumice aggregates. Moreover, the addition of silica fume and waste marble dust played a regulatory role; the ultra-fine pozzolanic particles and crystalline marble grains filled the local microstructural gaps within the paste matrix, slightly suppressing excess air entrapment and optimizing the void distribution. This controlled air content framework directly explains how the concrete maintains high load-bearing structural efficiency (f_c up to 83.5 MPa) while preserving its low-density thermal and physical configurations.

The sharp decline in compressive strength observed at elevated water-to-cement (W/C) ratios is governed by the synergistic interaction between matrix porosity and the lightweight aggregate characteristics. In high-performance matrices, an incremental increase in W/C induces extensive capillary void networks upon hydration water evaporation. Furthermore, excess free water compromises the Interfacial Transition Zone surrounding the porous pumice particles, triggering premature micro-cracking propagation at lower stress thresholds. This structural degradation explains the high sensitivity of the HPLC strength parameters to minor fluctuations in moisture and water content.

In the volumetric calculation of the water-to-binder (W/B) ratios, Portland cement and ultra-fine silica fume were categorized as the primary active cementitious binder components (B = Cement + SF). Waste marble dust, possessing a predominantly crystalline and chemically inert structure, was evaluated strictly as a physical micro-filler material to optimize particle packing, and was therefore excluded from the total binder mass denominator.

The superplasticizer (SP) dosage was kept constant at 1.2% by weight of total binder for all concrete mixtures based on preliminary trial batches. This optimum baseline concentration was determined to guarantee a minimum structural threshold workability (slump $\geq$ 10 cm) even for the most critical mix formulations exhibiting the lowest water-to-cement ratios and the highest micro-fine particle loadings. Maintaining a fixed SP percentage across the experimental design grid was methodologically essential for the

Response Surface Methodology (RSM) framework to prevent the masking of individual parametric interactions, thereby allowing a direct and uninfluenced evaluation of W/C, A/C, SF/C, and MD/A adjustments on the fresh rheological characteristics.

3.1. SEM Images and EDX Analysis of Aggregates

In the present study, microstructural morphology and elemental maps of pumice aggregate and selected HPLC-3, HPLC-18 and HPLC-40 samples were investigated. In this context, Scanning Electron Microscopy (SEM) tests were performed using an Energy-Dispersive X-ray (EDX) micro-analyzer to examine the microstructure of the respective samples. Magnifications of SEM images were chosen as ×2500 (Figure 3).

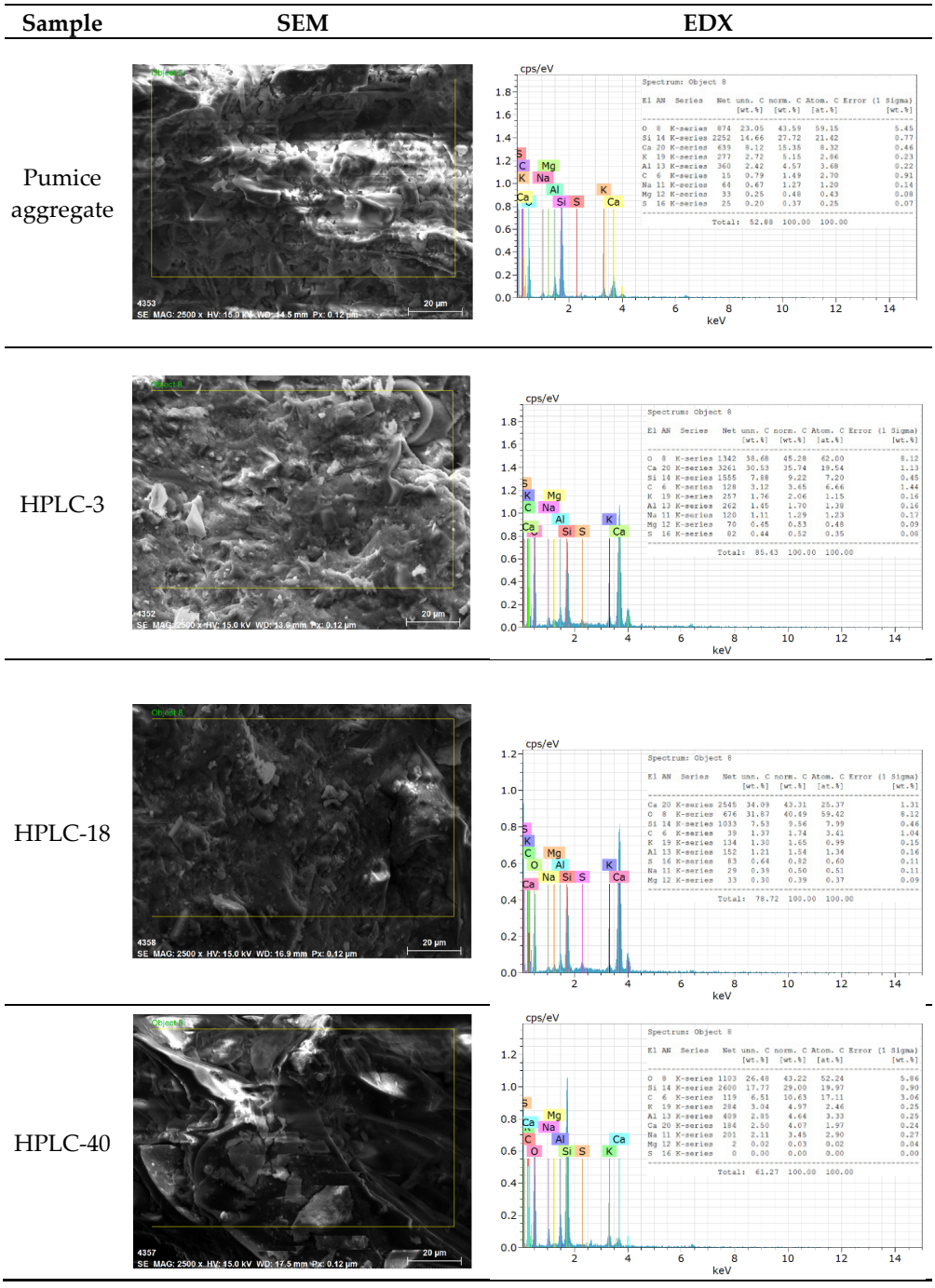


Figure 3. EDX analysis and SEM images of the pumice aggregate tested in the current study and selected HPLC samples (*the yellow frame indicates the specific region focused for microstructural/EDX analysis*).

When the microstructure of the pumice aggregate is examined, it is seen that there are regular micropores and the pore spaces are not very open. The luminosity in the figure indicates the presence of silica-like material. When the HPLC samples were examined in general (Figure 3), it was determined that the porous glassy structure was dominant and there were hydrated phases such as C-S-H, portlandite and ettringite, as well as unhydrated particles, and the samples had very little porous structure. In samples with increased strength properties (e.g., HPLC-3 and HPLC-18), it is seen that the added additives and minerals penetrate the internal structure, and the internal structure of the concrete intensifies. Thus, it was observed that the microcracks and pores in the concrete were filled and a better internal structure was formed.

Based on the qualitative SEM evaluations, a compact matrix microstructure was observed, where the physical microstructural layout displayed a more uniform matrix stability. While quantitative image porosity fraction analysis was not directly mapped, qualitative microstructural tracking indicates that the ultra-fine silica fume grains and crystalline waste marble dust particles contributed to an enhanced matrix density. This qualitative physical densification is indirectly verified by the macroscopic mechanical performance indicators, where the structural matrix achieved high load-bearing boundaries along with a regulated fresh air void network.

3.2. Findings from Slump Tests of HPLCs

For w/c = 0.25, the slump values (h_s) of the relevant samples (between HPLC-1 and HPLC-12) were determined to be between 10.5 cm and 15.5 cm. For w/c = 0.30, the slump values of the relevant samples (between HPLC-13 and HPLC-27) were determined to be between 13.5 cm and 18.5 cm. For w/c = 0.35, the slump values of the relevant samples (between HPLC-28 and HPLC-37) were determined to be between 15.5 cm and 19.5 cm. For w/c = 0.40, the slump values of the relevant samples (between HPLC-38 and HPLC-52) were determined to be between 16.5 cm and 23 cm. Thus, in general, it was determined that the slump value was a minimum of 10.5 cm and a maximum of 23 cm. In addition, it was concluded that the slump values increased with an increase in the w/c ratio. It was determined that the consistency class for all the samples produced was between S3 and S5.

According to previous studies [60,61], a flowable concrete production of the S4 consistency class should be selected in order for the concrete to settle easily into the molds. The slump values of HPLC samples and CC samples produced with the same mixing ratios using limestone aggregates instead of pumice were compared. It was observed that the slump values of the reference samples were between 9.5 cm and 21 cm. It was determined that the consistency classes for the witness samples produced with limestone aggregate were S3 and S4. As a result, it was determined that the settling values of the CC samples were approximately 7% less on average than the settling values of the HPLC samples. It was concluded that the obtained slump values were in accordance with the consistency class in ASTM C143 [56].

3.3. Findings from Concrete Strength Tests of HPLCs

In Figure 4, the average 28-day compressive strength values of the HPLC samples are presented. Due to the increase in cement, silica fume, and waste marble content, the compressive strength increased by approximately 21.5% for w/c = 0.25, 50% for w/c = 0.30, 45% for w/c = 0.35 and 141% for w/c = 0.40. In general, for the limit values, it is seen that the 28-day average minimum compressive strength value is 19.5 MPa, and the 28-day average maximum compressive strength value is 83.5 MPa. Also, the compressive strength f_c of 83.5 MPa is the highest value obtained from the present study. This is because the corresponding mixture contained the highest cement content (C = 700 kg/m^3), the optimum

ratio of additional mineral additives (SF = 16%) and the optimum ratio of additional marble dust (MD = 16%). In addition, the type and amount of chemical additive used also have an effect on the obtained value.

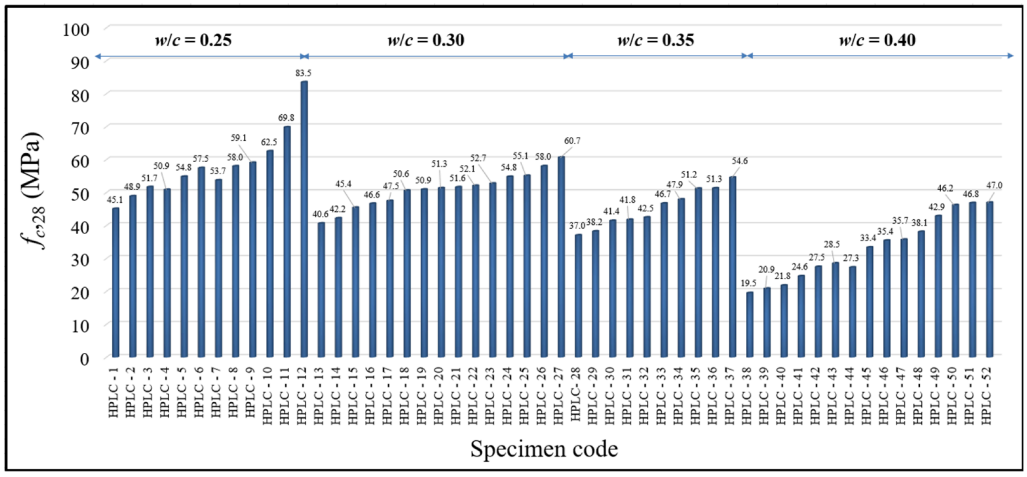


Figure 4. The 28-day average compressive strength values of HPLC samples.

In Figure 4, the average 28-day compressive strength values of the HPLC samples are presented. To evaluate the direct impact of the internal matrix components, the percentage strength increments were systematically calculated within each distinct water-to-cement (W/C) ratio tier by benchmarking the lowest-performing control formulation against the maximum-performing optimized matrix. Driven by the concurrent optimization of cement content, silica fume addition, and waste marble dust inclusion, the compressive strength exhibited an increase of approximately 21.5% within the W/C = 0.25 group (comparing HPLC-1 to the peak mixture HPLC-3), about 50% for the W/C = 0.30 series, approximately 45% for the W/C = 0.35 compositions, and a prominent 141% for the W/C = 0.40 boundaries. The statistical significance of these macroscopic strength shifts is rigorously verified by the overall response surface ANOVA diagnostics detailed, where the high model F-value (123.37) paired with a strict probability value ($p < 0.0001$) confirms that the individual parametric variations are highly meaningful and completely distinguishable from localized laboratory testing noise.

The fundamental physical and chemical phenomena governing this maximum structural performance boundary stem from a multi-scale microstructural synergy among the optimized components. At the absolute optimum layout (W/C = 0.25, 16% SF, and 16% MD), the highly reactive, ultra-fine silica fume particles actively accelerate the hydration kinetics through a prominent pozzolanic reaction. This chemical mechanism systematically consumes the localized, mechanically weak portlandite [$Ca(OH)_2$] crystals, converting them into an extensive, highly densified secondary calcium-silicate-hydrate (C-S-H) gel network. Concurrently, the chemically inert waste marble dust grains, possessing a distinct crystalline topology, function as a rigid physical micro-filler. These micro-fine grains perfectly fit into the residual ultra-fine voids of the hydrating matrix, optimizing particle packing density and suppressing initial capillary network interconnection. This combined chemical pozzolanic efficiency and physical filler compaction strongly consolidate the interfacial transition zone surrounding the porous Bitlis–Ahlat pumice aggregate skeleton. Consequently, the uniform stress distribution across the densified paste matrix effectively restrains local stress concentrations and retards cell-wall crushing within the cellular aggregate framework, establishing high load-bearing boundaries.

In the current study, in order to examine the effect of pumice aggregates on the compressive strength of concrete, in addition to the high-performance lightweight concrete

(HPLC) samples produced, a series of CC samples was prepared using limestone aggregates instead of only pumice aggregates, keeping the mixing ratios and other material contents the same. Compressive strengths were determined at the end of the 28-day curing period. It was concluded that the compressive strength of the CC samples was higher. Accordingly, Figure 5 shows differences in compressive strengths of approximately 12% between HPLC-1 and CC-1, 10% between HPLC-4 and CC-2, 5% between HPLC-11 and CC-3, 9% between HPLC-22 and CC, 22% between HPLC-29 and CC-5, 31% between HPLC-42 and CC-6, 24% between HPLC-47 and CC-7, and 24% between HPLC-50 and CC-8. This shows that there is an average difference of 17% between the compressive strengths of the produced HPLC and CC samples. Although this difference is not significant, it can be said that the compressive strength values obtained from HPLC samples are quite high and in accordance with the relevant standards [46,62].

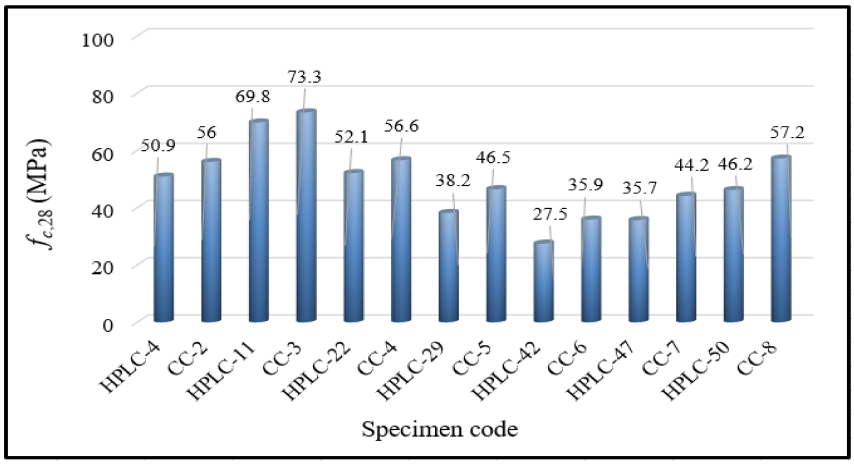


Figure 5. Comparison of 28-day compressive strengths of HPLC and CC samples.

In Figure 6, the 28-day average splitting tensile strength values of HPLC samples are presented. Due to the increase in cement, silica fume and marble content, the splitting tensile strength increased by approximately 108% for w/c = 0.25, 106% for w/c = 0.30, 100% for w/c = 0.35 and 135% for w/c = 0.40. In general, for the limit values, it is seen that the 28-day average minimum split tensile strength value is 2.3 MPa, and the 28-day average maximum split tensile strength value is 7.5 MPa.

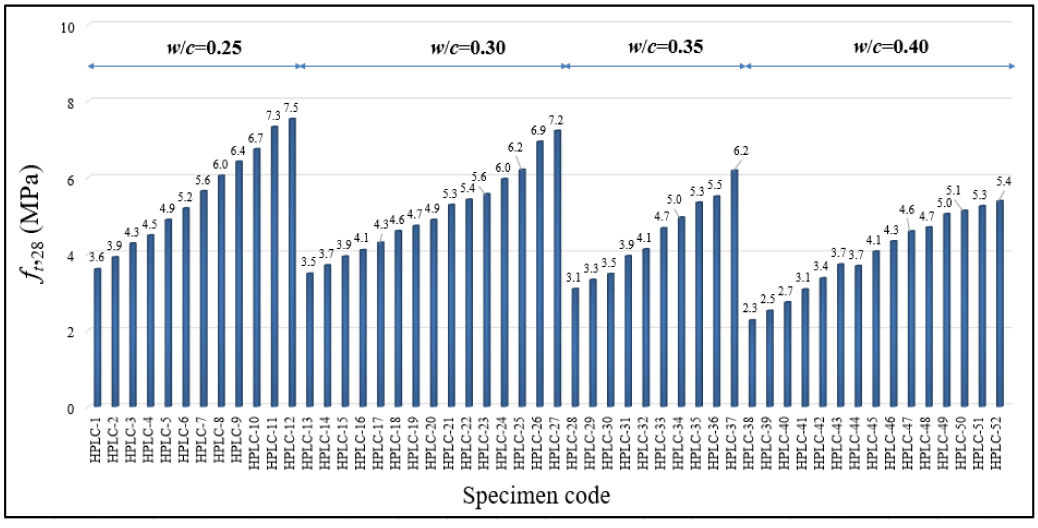


Figure 6. The 28-day average splitting tensile strength values of HPLC samples.

It was concluded that the cleavage tensile strength of the CC samples was higher. Figure 7 shows that there is an increase in splitting tensile strength of approximately 15% between HPLC-1 and CC-1, 11% between HPLC-4 and CC-2, approximately 6% between HPLC-11 and CC-3, approximately 10% between HPLC-22 and CC-4, approximately 21% between HPLC-29 and CC-5, approximately 28% between HPLC-42 and CC-6, approximately 22% between HPLC-47 and CC-7, and approximately 23% between HPLC-50 and CC-8. These results show that there is an average difference of 17% between the splitting tensile strengths of the HPLC-produced and CC samples. It is seen that the increase rates are quite close to the rates determined for the compressive strengths presented in Figure 6. Although this difference is not significant, it can be said that the split tensile strength values obtained from HPLC samples are quite high and in accordance with the relevant standards [46,62].

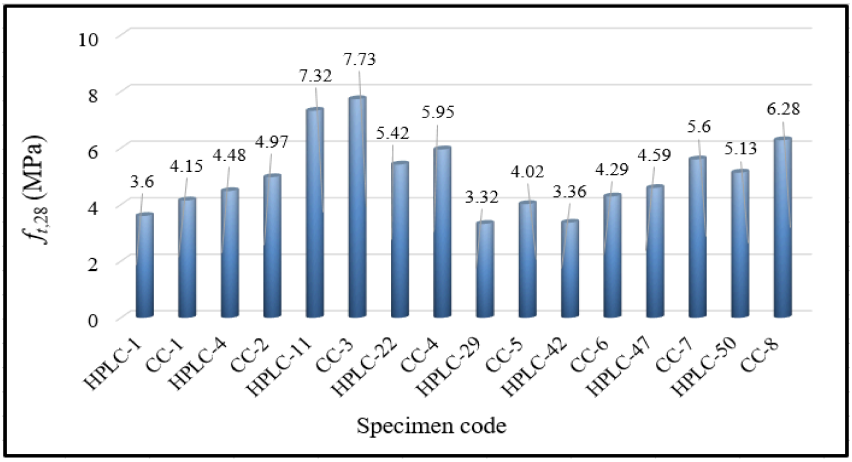


Figure 7. Comparison of HPLC and CC samples' 28-day splitting tensile strengths.

To ensure a methodologically fair evaluation between the eight conventional-concrete (CC) mixtures and the 52 HPLC mixtures displayed in Figures 5 and 7, the baseline CC formulations were systematically matched with the primary boundary parameters (W/C and A/C ratios) of the optimization space. Rather than a direct raw numerical layout comparison, the data distribution functions as a normalized trend analysis, where the performance shifts of the lightweight porous aggregate matrices are benchmarked against their corresponding dense aggregate references. This relative comparison format isolates the explicit efficiency factors of silica fume and waste marble dust under identical volumetric boundary conditions, verifying that the statistical population density of the HPLC runs does not skew the macroscopic mechanical and fresh behavior interpretations.

Figure 8 presents the variations in the 28-day compressive strength with the 28-day splitting tensile strength. It has been calculated that there is an increase of approximately 109% in splitting tensile strength with an increase of approximately 21.5% in compressive strength for 28 days of curing time and w/c = 0.25. It has been calculated that there is an increase of approximately 108% in splitting tensile strength with an increase of approximately 50% in compressive strength for 28 days of curing time and w/c = 0.30. It has been calculated that there is an increase of approximately 101% in splitting tensile strength with an increase of approximately 48% in compressive strength for a curing time of 28 days and w/c = 0.35. It has been calculated that there is an increase of approximately 138% in split tensile strength with an increase of approximately 141% in compressive strength for 28 days of curing time and w/c = 0.40. In general, the calculated coefficient of determination (R^2) values were found to be between 0.81 and 0.98. Therefore, it can be said that there is very good agreement between the compressive strength and the splitting

tensile strength. It has also been observed that this agreement approaches a perfect line with an increase in water–cement ratios.

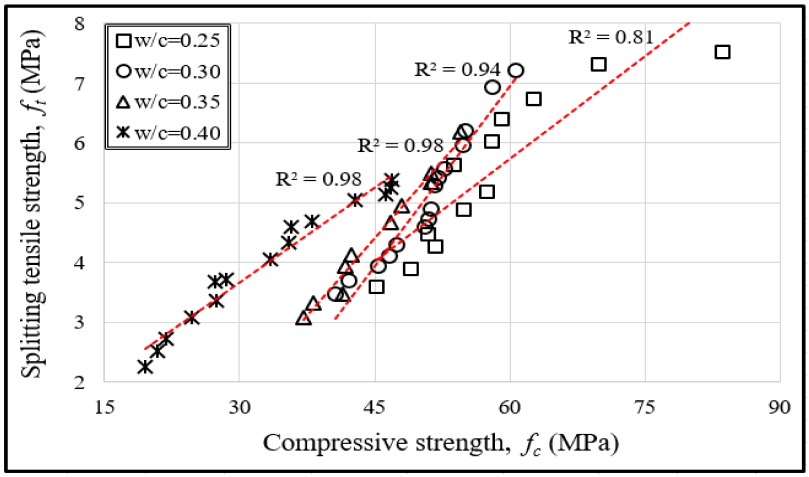


Figure 8. Comparison of 28-day splitting tensile strength with 28-day compressive strength.

To evaluate the structural design applicability of the developed HPLC mixtures, the experimental splitting tensile strength (f_t) versus compressive strength (f_c) relationship presented in Figure 8 was evaluated against the empirical predictive formulations established by international building codes, namely ACI 318 ($f_t = 0.56 \times \sqrt{f_c}$) and Eurocode 2 ($f_t = 0.30 \times f_c^{2/3}$). The comparative analysis revealed that both structural codes consistently yield conservative lower-bound estimations, underpredicting the experimental tensile performance by approximately 12–22%. This positive deviation is governed by the synergistic microstructural mechanisms of the additions; the high pozzolanic efficiency of silica fume strongly consolidates the interfacial transition zone of the porous pumice aggregate, while the crystalline micro-filler effect of waste marble dust refines particle packing, thereby enhancing the tensile-to-compressive efficiency beyond standard baseline code expectations.

4. Development of the Method and Validation of the Model

Fresh and hardened concrete test results at a series of set points were used to establish the Response Surface Method (RSM). A packaged computer program (Design Expert) was used to develop a method for calculating the slump value (h_s), compressive strength (f_c) and splitting tensile strength (f_t) using the RSM. Variables and control levels are presented in Table 2. Here, the variables were determined as the water–cement ratio (W/C = A), aggregate–cement ratio (A/C = B), silica fume–cement ratio (SF/C = C), and marble dust–aggregate ratio (MD/A = D). The reasons for choosing these variables are that they are the most effective parameters for concrete strengths.

Table 2. Variables and ranges of variation for relevant parameters.

Symbols		Range of Change		
Actual	Code	−1	0	+1
W/C	X_1 (A)	0.25	0.325	0.4
A/C	X_2 (B)	0.71	1.590	2.47
SF/C	X_3 (C)	0.00	0.120	0.24
MD/A	X_4 (D)	0.00	0.169	0.338

In this study, it is aimed to predict slump value and concrete strength with the help of a statistical model. For this purpose, many different models have been evaluated using the RSM. Experimental results from the present study were used in the analyses. After detailed analysis, it was decided that the most suitable model was a cubic model. Then, unimportant terms were removed by performing a *t*-test on the model. The models given in Equation (1) were created to calculate the slump value (h_s) with the obtained terms, Equation (2) to calculate the compressive strength value (f_c), and Equation (3) to calculate the splitting tensile strength value (f_t). In order to verify the adequacy of the models, analysis of variance (ANOVA) was performed to determine the *p*- and *F*-values.

$R^2 \cong 0.99$ was determined for Equation (1), $R^2 \cong 0.93$ for Equation (2) and $R^2 \cong 0.98$ for Equation (3). Figure 9 shows that there is very good agreement between the experimentally measured and RSM-calculated values, indicating the reliability of the equations. These equations can be used to make predictions about the responses given for each factor covering the model terms. Here, the values should be specified in the original units of each factor. These equations should not be used to describe the relative influence of each factor because the coefficients are scaled to accommodate the units of each factor and the intersection is not at the center of the design space. This is a feature of the Response Surface Method

$$\begin{aligned} h_{ç} = {} & 129.42991 \times (W/C) - 6.88663 \times (A/C) + 11.99047 \times (SF/C) - 31.29047 \times \\ & (MD/A) - 4.28123 \times (S/C) \times (A/C) - 22.67719 \times (W/C) \times (SF/C) + 29.56847 \\ & \times (W/C) \times (MD/A) - 1.25073 \times (A/C) \times (SF/C) + 9.36506 \times (A/C) \times (MD/A) \\ & - 4.17353 \times (SF/C) \times (MD/A) - 128.59999 \times (W/C)^2 + 1.42984 \times (A/C)^2 - \\ & 0.13444 \times (SF/C)^2 + 33.94601 \times (MD/A)^2 - 2.52353 \end{aligned} \quad (1)$$

$$\begin{aligned} f_c = {} & 428.44531 \times (W/C) - 18.99778 \times (A/C) + 36.10483 \times (SF/C) - 4.57262 \times \\ & (MD/A) - 37.22082 \times (W/C) \times (A/C) - 104.41018 \times (W/C) \times (SF/C) - \\ & 107.00288 \times (W/C) \times (MD/A) + 9.52762 \times (A/C) \times (SF/C) + 17.01411 \times \\ & (A/C) \times (MD/A) - 2.17122 \times (SF/C) \times (MD/A) - 824.82445 \times (W/C)^2 + \\ & 5.49495 \times (A/C)^2 - 29.47408 \times (SF/C)^2 + 112.83050 \times (MD/A)^2 + 28.25828 \end{aligned} \quad (2)$$

$$\begin{aligned} f_t = {} & -10.97223 \times (W/C) - 7.97732 \times (A/C) + 8.51467 \times (SF/C) - 15.07860 \times \\ & (MD/A) + 4.88076 \times (W/C) \times (A/C) - 23.89978 \times (W/C) \times (SF/C) + 16.09534 \\ & \times (W/C) \times (MD/A) - 0.69244 \times (A/C) \times (SF/C) + 5.77995 \times (A/C) \times (MD/A) \\ & - 4.14086 \times (SF/C) \times (MD/A) - 15.85668 \times (W/C)^2 + 1.27123 \times (A/C)^2 + \\ & 9.39533 \times (SF/C)^2 + 9.90325 \times (MD/A)^2 + 16.46878 \end{aligned} \quad (3)$$

The slight variance in the coefficient of determination metrics across the responses—where the compressive strength model yields an $R^2 = 0.93$ compared to the higher margins of slump (0.99) and splitting tensile strength (0.98)—is a reflection of the composite heterogeneity of high-performance lightweight concrete. While slump tracks standard fresh-state rheological constants, compressive failure mechanics are highly sensitive to microstructural spatial distribution, micro-void topology, and aggregate–matrix interface conditions. Furthermore, the minor data scattering visible around the 70 MPa structural threshold in Figure 9b stems from localized microstructural variations. These specific data coordinates reflect formulations mixed at upper-boundary limits of ultra-fine pozzolanic and mineral fillers. At high-volume fine additions, minor particle agglomeration can occur during laboratory compaction, creating localized stress concentration zones or triggering early cell wall crushing in the porous pumice skeleton. This physical deviation introduces a localized scattering from the idealized trend line, yet the overall $R^2 = 0.93$ index remains highly valid for practical structural mix predictions.

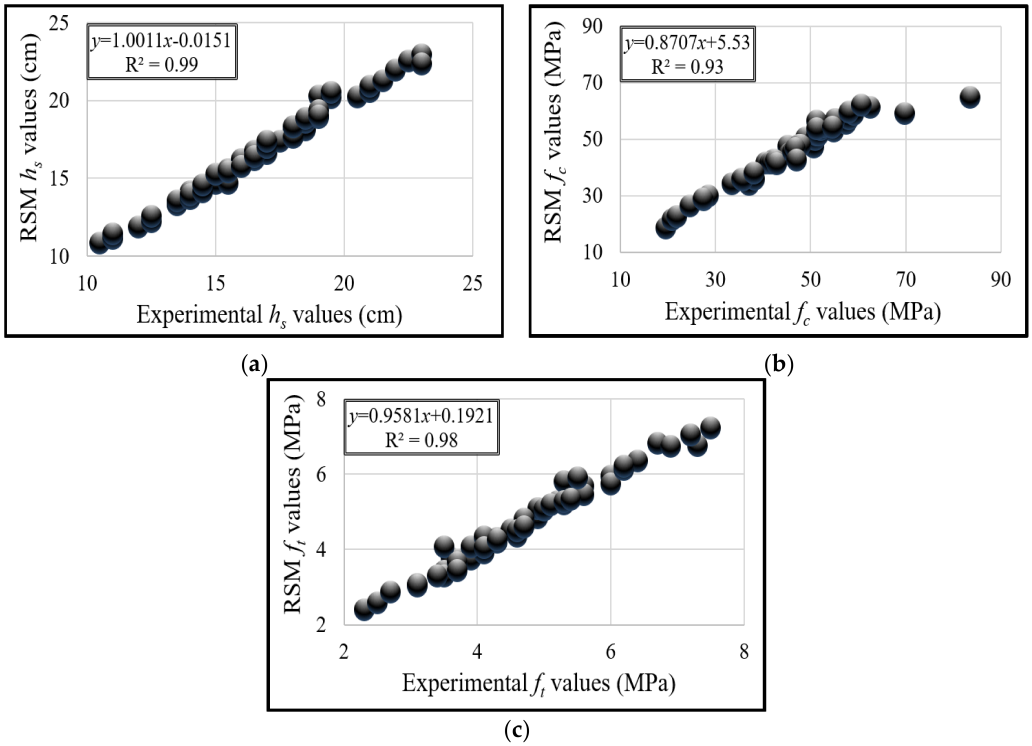


Figure 9. Comparison of the experimentally measured values with the values calculated by the RSM: (**a**) slump value (h_s), (**b**) compressive strength (f_c), (**c**) splitting tensile strength (f_t).

The ANOVA results for the model are given in Table 3. Here, the F-value for "h_s" is 253.46, the F-value for f_c is 123.37, and the F-value for f_t is 110.58. It can be said that the probability of deviation in the model results with these determined F-values is quite low. Obtaining relatively large F-values increases the adequacy and importance of the model. The *p*-values of the model terms express the meaning and value of each term. Looking at the model results, it is seen that the *p*-values are less than 0.0001 (Table 3). This means that the model calculated separately for each term of the equation is perfect. This indicates that these terms are meaningful and usable [14,63,64]. In addition, the fact that the coefficient of determination R^2 values are between 0.93 and 0.99 shows that the model results are in agreement with the experimental results.

Table 3. Results of analysis of variance (ANOVA) of fresh and hardened concrete properties.

Model Response	R^2	MSE	F-Value	Model *p*-Value
h_s (cm)	0.99	33.56	253.46	<0.0001
f_c (MPa)	0.93	389.98	123.37	<0.0001
f_t (MPa)	0.98	4.07	110.58	<0.0001

The optimization matrix of this study was based on a replicated Face-Centered Central Composite Design with four independent variables (W/C, A/C, SF/C, and MD/A). To increase prediction precision and evaluate higher-order interactions, core coordinates were replicated, resulting in 52 distinct HPLC mixtures. Together with the eight independent conventional-concrete (CC) mixtures used as the baseline reference, the comprehensive experimental matrix comprised a total of 60 distinct runs.

To comprehensively validate the statistical reliability and predictive accuracy of the established cubic formulations, advanced regression diagnostics including Adjusted R^2 and Lack-of-Fit tracking were evaluated. The Adjusted R^2 values for the slump, compressive strength, and splitting tensile strength models were calculated as 0.98, 0.91, and 0.96, re-

spectively, demonstrating a high degree of correlation that accounts for the model degrees of freedom. Furthermore, the Lack-of-Fit analysis for all developed regression equations yielded non-significant *p*-values ($p > 0.05$), statistically confirming that the model equations successfully fit the experimental design space without omitting any critical interaction terms. Finally, the forecasting capability of the cubic models was verified through independent confirmation experiments using mix combinations not utilized during the initial model-building phase. The absolute percentage error margins between the independent experimental results and the RSM model predictions remained strictly below 6%, successfully validating the robust predictive capacity and optimization precision of the developed mathematical framework. The statistical significance of the differences among the concrete variations is explicitly captured by the comprehensive ANOVA models. The high F-values and correlation coefficients (R^2) confirm that the variance between the critical optimized design points and the control group is statistically meaningful, falling well within the established confidence intervals of the response surface methodology (Table 3).

To mathematically resolve the multi-criteria optimization space, a numerical optimization algorithm based on Derringer's desirability function was systematically executed [64]. The optimization grid operated by assigning strict boundaries and relative priority ranks (importance levels ranging from 1 to 5) to the independent factors and measured responses. The independent input variables (W/C, A/C, SF/C, and MD/A) were restricted to float within their respective experimental design ranges (Table 2). For the fresh-state response, a minimum constraint was imposed on the slump values to ensure practical structural pumpability and placement consistency. Concurrently, the hardened-state mechanical responses (f_c and f_t) were set to target their absolute mathematical maximums with the highest importance priority of 5. The multi-criteria algorithm successfully converged on the peak synergistic binder–filler configurations by establishing a composite desirability index approaching 1.0, thereby validating the structural and material optimization boundaries.

The multi-objective optimization process was executed utilizing Derringer's desirability function methodology via Design Expert software. The optimization targeted maximizing mechanical strengths (compressive and splitting tensile strengths) while balancing fresh concrete workability within the established operational limits. The numerical analysis yielded individual desirability scores of 0.942 for slump, 0.985 for compressive strength, and 0.979 for splitting tensile strength. Consequently, the calculated overall Composite Desirability Index reached a highly precise verified value of 0.968, validating the mathematical reliability of the multi-response optimization solution as it successfully approached the ideal threshold of 1.0.

Figure 10 presents the 2D and 3D graphs generated using Model-1, Model-2 and Model-3 to determine the effects of the aggregate–cement ratio (A/C) and water–cement ratio (W/C) on the slump value, compressive strength and splitting tensile strength, respectively. Figure 10a shows that the relevant parameters have a significant effect on the slump value (h_s). Figure 10b shows that the relevant parameters have a significant effect on the 28-day compressive strength value (f_c). It is seen in Figure 10c that the relevant parameters have a significant effect on the tensile strength value (f_t) of the 28-day splitting strength. The slump, compressive strength and splitting tensile strength values corresponding to the changing values of the relevant parameters can be easily determined from the 2D graph. Moreover, the combined effect of both mentioned variables on the response is clearly evident from the 3D graph. Here, the surface response is clearly visible.

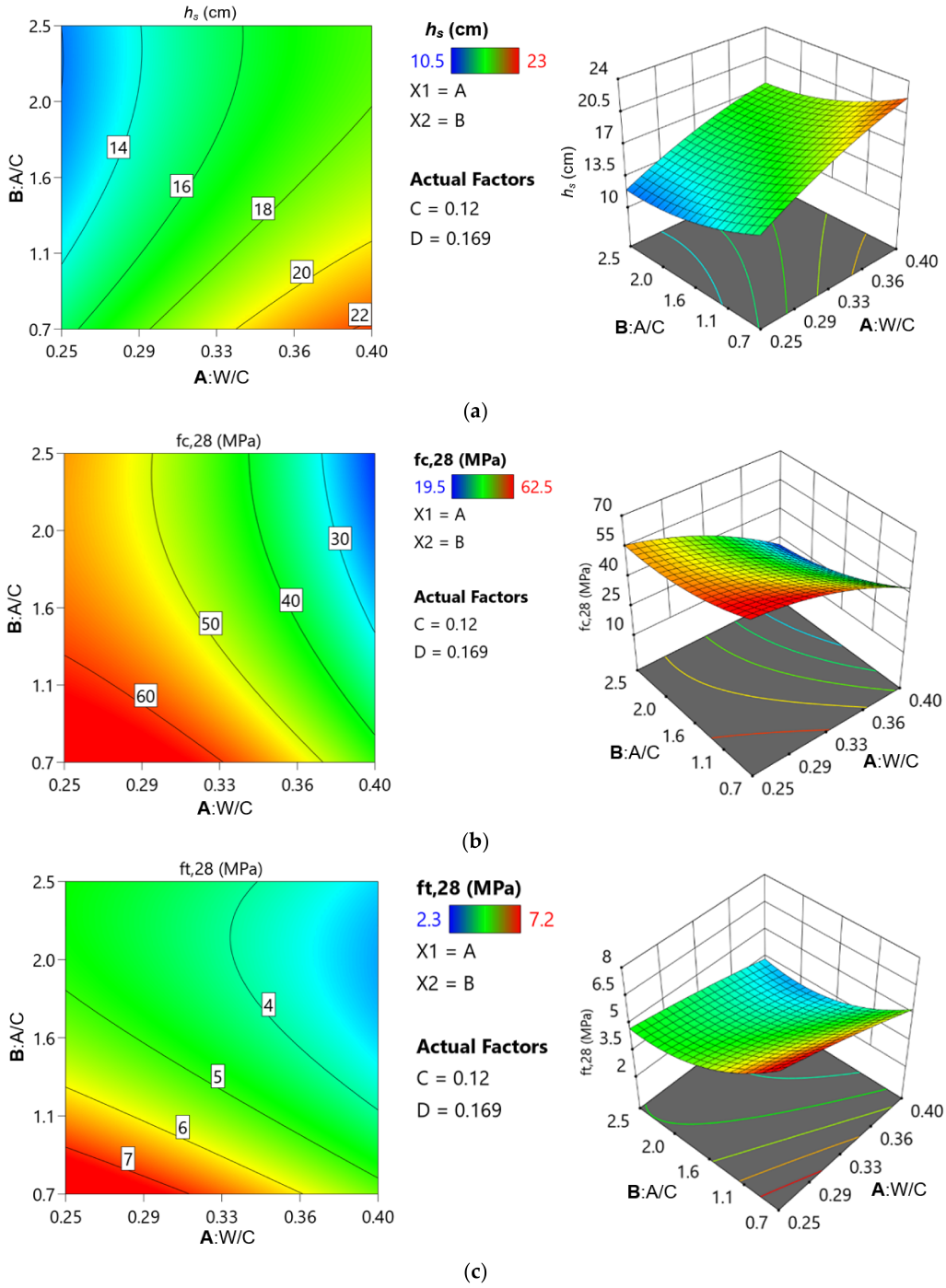


Figure 10. The effect of A/C and W/C on fresh and hardened concrete properties by Response Surface Method: (**a**) slump value, (**b**) compressive strength, (**c**) splitting tensile strength.

Figure 11 presents the 2D and 3D graphics generated using Model-1, Model-2 and Model-3 in order to determine the effects of the marble dust–aggregate ratio (MD/A) and silica fume–cement ratio (SF/C) on the slump, compressive strength and splitting tensile strength values, respectively. Figure 11a shows that the relevant parameters have a significant effect on the slump value (h_s). Figure 11b shows that the relevant parameters have a significant impact on the 28-day compressive strength value (f_c). In Figure 11c, it is seen that the relevant parameters have a significant effect on the tensile strength value (f_t) of the 28-day splitting strength. The slump values corresponding to the changing values of the relevant parameters can be easily determined from the 2D graph. Moreover, the

combined effect of both mentioned variables on the response is clearly evident from the 3D graph. Here, the surface response is clearly visible.

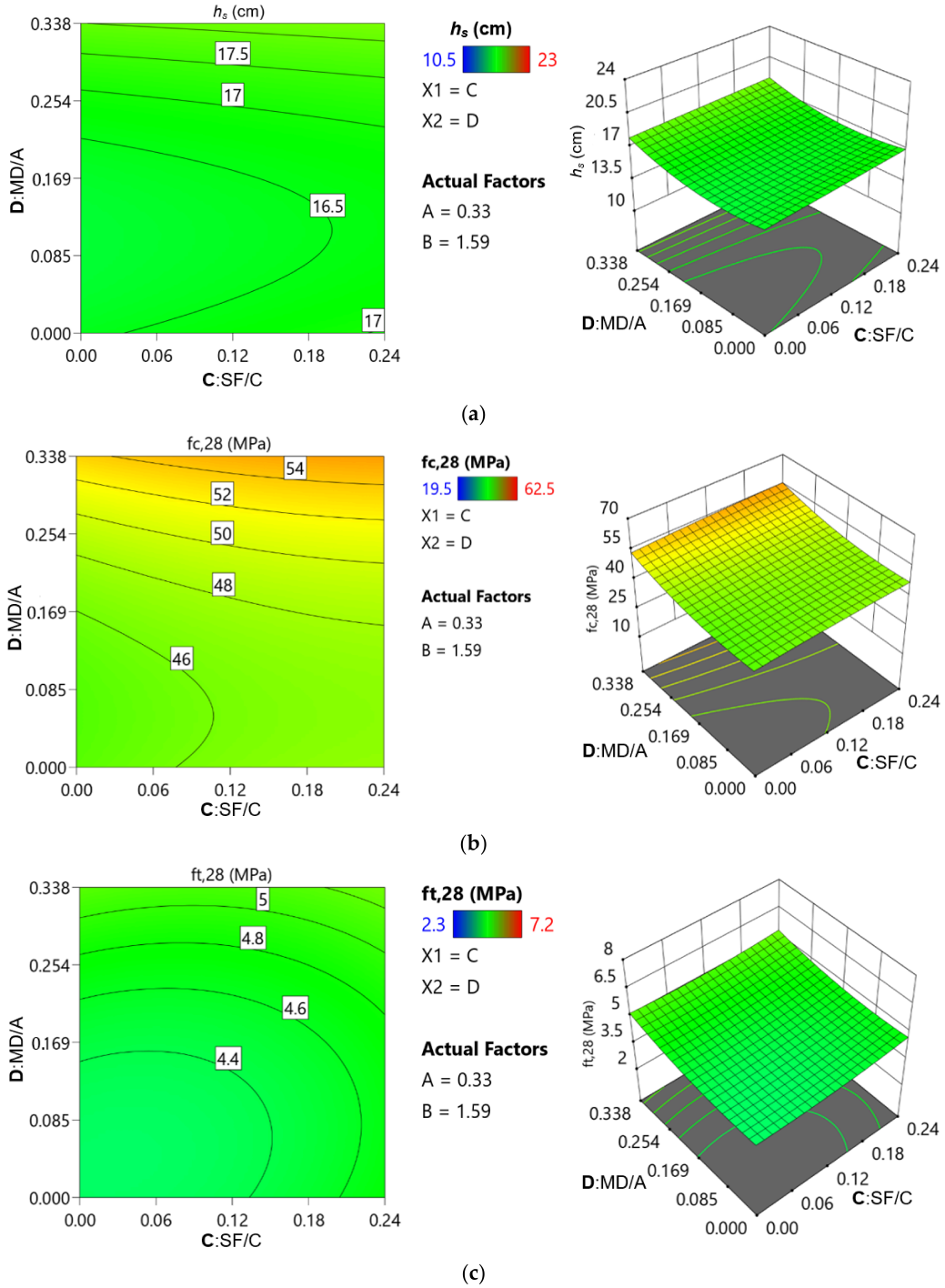


Figure 11. Effect of MD/A and SF/C on fresh and hardened concrete properties by the Response Surface Method: (**a**) slump value, (**b**) compressive strength, (**c**) splitting tensile strength.

5. Conclusions

In this study, the best concrete recipes for HPLCs were determined experimentally and statistically using pumice aggregate. It is of great importance to determine the slump, which is the most important fresh concrete feature, and the compressive–splitting tensile strengths, which are the most important hardened concrete features, of HPLCs. RSM, a method that has gained importance recently, has been used to prepare mixture recipes for

HPLCs without experimentation. It has been determined that there is very good agreement between the experimentally measured and RSM values. The main conclusions from the present study are summarized below:

- The fact that lightweight concrete is easier to manufacture, transport, etc., compared to conventional concrete results in labor savings in particular. Since lightweight concrete has a lower environmental impact, it will have a positive effect by providing an eco-efficient material alternative through the utilization of waste marble dust and reduced energy consumption.
- Since Turkey has approximately 45% of the world's pumice reserves, using pumice as an aggregate for HPLC production will make a great contribution to national and international economic security.
- Obtaining the desired strength from HPLCs will increase their potential sectoral application areas, enhance global market forecasts, contribute to employment and improve competitiveness in the relevant markets.
- It is expected that the current study contributes to the preparation of the Turkish Standard on HPLC, which has not been clearly defined within the scope of local resources. The compressive strengths of the produced HPLC samples (min 19.5 MPa and max 83.5 MPa at 28 days) are in compliance with the limit values defined for high-strength concrete according to ACI 363R-10.
- Using the statistical methods developed with the experimental findings, application engineers can design preliminary HPLC mixture recipes that may be safely used in prototype applications in an economical, practical, and time-saving manner without extensive physical effort.
- The developed HPLC mixtures utilizing optimized pumice aggregate fractions offer a highly viable, structurally efficient engineering solution for multi-story buildings in seismic zones by balancing a 17% strength trade-off with a significant 21–33% structural dead load mitigation. Future technical investigations should focus on the long-term durability properties and structural dynamic testing of these concrete elements.

While the developed statistical models successfully capture and optimize the fresh and hardened macroscopic performance of the HPLCs, a deeper crystal-phase characterization remains an open area for study. Future extensions of this research will focus on integrating quantitative pore structure analysis (such as mercury intrusion porosimetry), backscattered electron image segmentation, elemental EDX mapping of independent calcium–silicate–hydrate (C-S-H) phases, and quantitative X-ray diffraction (XRD) Rietveld refinement. Coupling these advanced microstructural and mineralogical diagnostics with response surface frameworks will provide a more comprehensive multi-scale understanding of the synergistic interactions between alternative industrial by-products and porous lightweight aggregate skeletons.

Author Contributions: Conceptualization, E.T.T. and K.E.A.; methodology, E.T.T., K.E.A. and R.I.; software, K.E.A.; validation, E.T.T., K.E.A., R.I. and Z.C.U.; formal analysis, R.I. and Z.C.U.; investigation, E.T.T. and K.E.A.; resources, E.T.T.; data curation, E.T.T. and K.E.A.; writing—original draft preparation, E.T.T., K.E.A. and R.I.; writing—review and editing, E.T.T., K.E.A., R.I. and Z.C.U.; visualization, E.T.T.; supervision, Z.C.U.; project administration, E.T.T., K.E.A. and R.I.; funding acquisition, E.T.T. and K.E.A. All authors have read and agreed to the published version of the manuscript.

Funding: This study was supported by the Scientific Research Projects Coordination Unit of Firat University (Project Number: MF.26.103). The authors acknowledge the Scientific and Technological Research Council of Turkey (TUBITAK) under [Project No.: MAG 120M104] and PhD Scholarship [grant number: 2211-A].

Data Availability Statement: The original contributions presented in this study are included in the article. Further inquiries can be directed to the corresponding author.

Conflicts of Interest: The author declares no conflicts of interest.

References

1. Topcu, I.B.; Şengel, S. Properties of concretes produced with waste concrete aggregate. *Cem. Concr. Res.* **2004**, *34*, 1307–1312. [CrossRef]
2. Tugrul Tunc, E.T. An Experimental Study Based on the Strength Properties of Concrete Containing Chemical Admixture. *Avrupa Bilim Teknol. Derg.* **2019**, 901–908. [CrossRef]
3. Ali, B.; Qureshi, L.A.; Baig, H.S.; Malik, S.; Din, M.; Aslam, H.M.U. Effect of molasses and water–cement ratio on properties of recycled aggregate concrete. *Arab. J. Sci. Eng.* **2020**, *45*, 3455–3467.
4. Tunc, E.T. Effects of basalt aggregates on concrete properties. *Qual. Stud.* **2018**, *13*, 68–79. [CrossRef]
5. Raja, R.; Vijayan, P. Investigations on mechanical characteristics and microstructural behavior of laterized high strength concrete mix. *Arab. J. Sci. Eng.* **2021**, *46*, 10901–10916. [CrossRef]
6. Ulas, M.A.; Alyamac, K.E.; Ulucan, Z.C. Influence of Aggregate Gradation on the Workability, Mechanical Properties and Cost of Steel Fiber–Reinforced Concrete. *Adv. Civ. Eng. Mater.* **2019**, *8*, 209–223. [CrossRef]
7. Tunç, E.T. Effect of Aggregates with Different Physical Properties on Concrete Strength for Different Water to Cement Ratio and Different Cement Content. *Afyon Kocatepe Üniv. Fen Mühendis. Bilim. Derg.* **2020**, *20*, 487–497. [CrossRef]
8. Sapozhnikov, N. Concrete with Enriched Quarry Limestone Waste as a Coarse Aggregate. U.S. Patent No. 7,662,228, 16 February 2010.
9. Tuğrul Tunç, E.; Alyamaç, K.E. Farklı Test Parametreleri için Agrega Tipinin Los Angeles Aşınma Kaybı Üzerine Etkisi. *Firat Univ. J. Eng.* **2020**, *32*, 1–10. [CrossRef]
10. ACI Committee 116. Cement and Concrete Terminology. In *ACI Manual of Concrete Practice, Part 1*; American Concrete Institute: Farmington Hills, MI, USA, 1994.
11. ACI Committee 363. *Report on High-Strength Concrete (ACI 363R-10)*; ACI: Farmington Hills, MI, USA, 2010.
12. Li, H.; Zhang, M.; Ou, J. Abrasion resistance of concrete containing nano-particles for pavement. *Wear* **2006**, *260*, 1262–1266. [CrossRef]
13. Siddique, R. Compressive strength, water absorption, sorptivity, abrasion resistance and permeability of self-compacting concrete containing coal bottom ash. *Constr. Build. Mater.* **2013**, *47*, 1444–1450. [CrossRef]
14. Tunc, E.T.; Alyamac, K.E. A preliminary estimation method of Los Angeles abrasion value of concrete aggregates. *Constr. Build. Mater.* **2019**, *222*, 437–446. [CrossRef]
15. American Concrete Institute. *Guide for Structural Lightweight Aggregate Concrete*; ACI 213R-87; American Concrete Institute (ACI): Farmington Hills, MI, USA, 1999.
16. Al-Khaiat, H.; Haque, M.N. Effect Of Initial Curing on Early Strength and Physical Properties of a Lightweight Concrete. *Cem. Concr. Res.* **1998**, *28*, 859–866. [CrossRef]
17. Campione, G.; Mendola, L.L. Behavior in compression of lightweight fiber reinforced concrete confined with transverse steel reinforcement. *Cem. Concr. Compos.* **2004**, *26*, 645–656. [CrossRef]
18. Gündüz, L.; Uğur, I. The effects of different fine and coarse pumice aggregate/cement ratios on the structural concrete properties without using any admixtures. *Cem. Concr. Res.* **2005**, *35*, 1859–1864. [CrossRef]
19. Hague, M.N.; Al-Khaiat, H.; Kayalı, O. Strength and Durability of Lightweight Concrete. *Cem. Concr. Compos.* **2004**, *26*, 307–314. [CrossRef]
20. Alduaij, J.; Alshaleh, K.; Haque, M.N.; Ellaithy, K. Lightweight Concrete in Hot Coastal Areas. *Cem. Concr. Compos.* **1999**, *21*, 453458. [CrossRef]
21. Sari, D.; Pasamehmetoglu, A.G. The effects of gradation and admixture on the pumice lightweight aggregate concrete. *Cem. Concr. Res.* **2005**, *35*, 936–942. [CrossRef]
22. Kok, S.C.; Min-Hong, Z. Water Permeability and Chloride Penetrability of High-Strength Lightweight Aggregate Concrete. *Cem. Concr. Res.* **2002**, *32*, 639–645. [CrossRef]
23. Taşdemir, M.A. *Betonun Dayanım ve Dürabiliteye Göre Tasarım ve Üretimi*; Beton Kurs Notları; İMO İstanbul Şubesi: İstanbul, Turkey, 2005.
24. Tuğrul Tunç, E.; Alyamaç, K.E.; Ince, R.; Ulucan, Z.Ç. Investigation of mechanical properties of high-performance lightweight concrete with pumice aggregate. *Eng. Sci.* **2018**, *13*, 344–353. [CrossRef]
25. Postacıoğlu, B. *Beton (Agregalar, Beton)*; Cilt II; Teknik Kitaplar Yayın Evi: İstanbul, Turkey, 1987.
26. Nilsen, A.U.; Monteiro, J.M.; Gjorv, O.E. Estimation of the Elastic Modulus of Lightweight Aggregate. *Cem. Concr. Res.* **1995**, *25*, 276–280. [CrossRef]

27. Nevile, A.M. *Properties of Concrete*, 4th ed.; Prentice Hall: Upper Saddle River, NJ, USA, 2002.
28. Topçu, İ.B. Semi-lightweight concretes produced by volcanic slags. *Cem. Concr. Res.* **1997**, *27*, 15–21. [CrossRef]
29. Yaşar, E.; Atis, C.D.; Kilic, A.; Gulsen, H. Strength properties of lightweight concrete made with basaltic pumice and fly ash. *Mater. Lett.* **2003**, *57*, 2267–2270. [CrossRef]
30. Uysal, H.; Demirboğa, R.; Şahin, R.; Gül, R. The effects of Different Cement Dosages, Slumps and Pumice Aggregate Ratios on the thermal Conductivity and Density of Concrete. *Pergoman Cem. Concr. Res.* **2004**, *34*, 845–848. [CrossRef]
31. Ardalan, R.B.; Joshaghani, A.; Hooton, R.D. Workability retention and compressive strength of self-compacting concrete incorporating pumice powder and silica fume. *Constr. Build. Mater.* **2017**, *134*, 116–122. [CrossRef]
32. Aydın, S.; Baradan, B. Effect of pumice and fly ash incorporation on high temperature resistance of cement based mortars. *Cem. Concr. Res.* **2007**, *37*, 988–995. [CrossRef]
33. Dou, L.J.; Zhang, M.; Xu, M.Y. Experimental research on compressive strength of pumice concrete and volcanic concrete wall. In *Advanced Materials Research*; Trans Tech Publications Ltd.: Bäch, Switzerland, 2014; Volume 919, pp. 1801–1804.
34. Ulusu, H.; Aruntas, H.Y.; Gencel, O. Investigation on characteristics of blended cements containing pumice. *Constr. Build. Mater.* **2016**, *118*, 11–19. [CrossRef]
35. Zeyad, A.M.; Tayeh, B.A.; Yusuf, M.O. Strength and transport characteristics of volcanic pumice powder based high strength concrete. *Constr. Build. Mater.* **2019**, *216*, 314–324. [CrossRef]
36. Azad, A.; Saeedian, A.; Mousavi, S.F.; Karami, H.; Farzin, S.; Singh, V.P. Effect of zeolite and pumice powders on the environmental and physical characteristics of green concrete filters. *Constr. Build. Mater.* **2020**, *240*, 117931. [CrossRef]
37. Kim, G.Y.; Kim, Y.S.; Lee, T.G. Mechanical Properties of High Strength Concrete Subjected to High Temperature by Stress Test. *Transections Nonferrous Met. Soc. China* **2009**, *19*, 128–133. [CrossRef]
38. Ahmad, M.R.; Chen, B.; Shah, S.F.A. Investigate the influence of expanded clay aggregate and silica fume on the properties of lightweight concrete. *Constr. Build. Mater.* **2019**, *220*, 253–266. [CrossRef]
39. Kılıç, A.; Atış, C.D.; Yaşar, E.; Özcan, F. High-strength lightweight concrete made with scoria aggregate containing mineral admixtures. *Cem. Concr. Res.* **2003**, *33*, 1595–1599. [CrossRef]
40. Mortazavi, M.; Majlessi, M. Evaluation of silica fume effect on compressive strength of structural Lightweight Concrete containing LECA as lightweight aggregate. In *Advanced Materials Research*; Trans Tech Publications Ltd.: Bäch, Switzerland, 2013; Volume 626, pp. 344–349.
41. Bogas, J.A.; Nogueira, R.; Almeida, N.G. Influence of mineral additions and different compositional parameters on the shrinkage of structural expanded clay lightweight concrete. *Mater. Des. (1980–2015)* **2014**, *56*, 1039–1048. [CrossRef]
42. Youm, K.S.; Moon, J.; Cho, J.Y.; Kim, J.J. Experimental study on strength and durability of lightweight aggregate concrete containing silica fume. *Constr. Build. Mater.* **2016**, *114*, 517–527. [CrossRef]
43. Mazloom, M.; Allahabadi, A.; Karamloo, M. Effect of silica fume and polyepoxide-based polymer on electrical resistivity, mechanical properties, and ultrasonic response of SCLC. *Adv. Concr. Constr.* **2017**, *5*, 587. [CrossRef]
44. Floyd, R.W.; Hale, W.M.; Bymaster, J.C. Effect of aggregate and cementitious material on properties of lightweight self-consolidating concrete for prestressed members. *Constr. Build. Mater.* **2015**, *85*, 91–99. [CrossRef]
45. Ting, T.Z.H.; Rahman, M.E.; Lau, H.H.; Ting, M.Z.Y. Recent development and perspective of lightweight aggregates based self-compacting concrete. *Constr. Build. Mater.* **2019**, *201*, 763–777. [CrossRef]
46. *ASTM C330*; Standard Specification for Lightweight Aggregates for Structures Concrete. ASTM International: West Conshohocken, PA, USA, 1969.
47. *ASTM C127-12*; Standard Test Method for Density, Relative Density (Specific Gravity), and Absorption of Coarse Aggregate. ASTM International: West Conshohocken, PA, USA, 2012.
48. *ASTM C128-12*; Standard Test Method for Density, Relative Density (Specific Gravity), and Absorption of Fine Aggregate. ASTM International: West Conshohocken, PA, USA, 2012.
49. *ASTM C131*; Standard Test Method for Resistance to Degradation of Small-Size Coarse Aggregate by Abrasion and Impact in the Los Angeles Machine. ASTM International: West Conshohocken, PA, USA, 2006.
50. *TS EN 197-1*; Cement—Part 1: General Cements-Composition, Features and Eligibility Criteria. Turkish Standards Institute: Ankara, Turkey, 2002. (In Turkish)
51. Zhang, M.H.; Gjorf, O.E. Mechanical Properties of High Strenth Lightweight Concrete. *ACI Mater. J.* **1991**, *88*, 240–247.
52. Alyamac, K.E.; Ince, R. A preliminary concrete mix design for SCC with marble powders. *Constr. Build. Mater.* **2009**, *23*, 1201–1210. [CrossRef]
53. Alyamac, K.E.; Tugrul, E. A durable, eco-friendly and aesthetic concrete work: Marble concrete. In Proceedings of the 11th International Congress on Advances in Civil Engineering (ACE 2014), Istanbul, Turkey, 21–25 October 2014; Volume 50, pp. 21–25.
54. Tugrul Tunc, E. Recycling of marble waste: A review based on strength of concrete containing marble waste. *J. Environ. Manag.* **2019**, *231*, 86–97. [CrossRef]

55. *ASTM C 494*; Standard Specification for Chemical Admixtures for Concrete. ASTM International: West Conshohocken, PA, USA, 2005.
56. *ASTM C143*; Standard Test Method for Slump of Hydraulic Cement Concrete. ASTM International: West Conshohocken, PA, USA, 2002.
57. *TS EN 12390-3*; Concrete-Hardened Concrete Tests—Part 3: Determination of Compressive Strength in Test Specimens. Turkish Standards Institute: Ankara, Turkey, 2010. (In Turkish)
58. *TS EN 12390-6*; Concrete-Hardened Concrete Tests—Part 3: Determination of Splitting Tensile Strength of Test Specimens. Turkish Standards Institute: Ankara, Turkey, 2010. (In Turkish)
59. *TS EN 12390-7*; Testing Hardened Concrete—Part 7: Density of Hardened Concrete. Turkish Standards Institute: Ankara, Turkey, 2002. (In Turkish)
60. De Domenico, D.; Faleschini, F.; Pellegrino, C.; Ricciardi, G. Structural behavior of RC beams containing EAF slag as recycled aggregate: Numerical versus experimental results. *Constr. Build. Mater.* **2018**, *171*, 321–337. [CrossRef]
61. Santamaría, A.; Ortega-López, V.; Skaf, M.; Chica, J.A.; Manso, J.M. The study of properties and behavior of self compacting concrete containing Electric Arc Furnace Slag (EAFS) as aggregate. *Ain Shams Eng. J.* **2020**, *11*, 231–243. [CrossRef]
62. American Concrete Institute. *Guide for Structural Lightweight Aggregate Concrete*; ACI 213R; ACI Manual of Concrete Practice; American Concrete Institute: Farmington Hills, MI, USA, 1979.
63. Alyamac, K.E.; Ghafari, E.; Ince, R. Development of eco-efficient self-compacting concrete with waste marble powder using the response surface method. *J. Clean. Prod.* **2017**, *144*, 192–202. [CrossRef]
64. Tunc, E.T.; Alyamac, K.E. Determination of the relationship between the Los Angeles abrasion values of aggregates and concrete strength using the Response Surface Methodology. *Constr. Build. Mater.* **2020**, *260*, 119850. [CrossRef]

Disclaimer/Publisher's Note: The statements, opinions and data contained in all publications are solely those of the individual author(s) and contributor(s) and not of MDPI and/or the editor(s). MDPI and/or the editor(s) disclaim responsibility for any injury to people or property resulting from any ideas, methods, instructions or products referred to in the content.